AIAA JOURNAL
Vol. 50, No. 10, October 2012

Rocket Noise Sources Localization Through a Tailored Beam-Forming Technique

Damiano Casalino* and Samuele Santini†
Centro Italiano Ricerche Aerospaziali, I-81043 Capua, Italy
Mariano Genito‡
European Launch Vehicle S.p.A., I-00034 Colleferro, Italy
and
Valerio Ferrara§
AVIO S.p.A., I-00034 Colleferro, Italy

DOI: 10.2514/1.J051479

A source localization and reconstruction technique is applied to analyze wall pressure measurements undertaken on the surface of a space launcher mock-up. The technique is based on the combined use of a beam-forming technique and elementary acoustic solutions tailored to the space launcher geometry. Two classes of acoustic elementary solutions are considered: plane waves impinging on the surface of an infinite cylinder computed analytically through a literature formula, and plane waves impinging on the real space launcher computed numerically through a computational acoustic technique. These two classes of basis functions are proven to provide consistent source localization results in the addressed frequency range. Moreover, the source reconstruction technique is shown to recover the measured wall pressure cross-spectra with a good confidence level in magnitude and fair confidence level in phase. The proposed launcher-tailored source localization and reconstruction techniques are therefore promising useful tools for the vibroacoustic design of future launch vehicles.

Downloaded by UNIVERSITY OF TENNESSEE on March 18, 2013 | http://arc.aiaa.org | DOI: 10.2514/1.J051479

Nomenclature

A_m, ϵ_m, γ_m	=	cylinder scattered wave coefficients
$\mathbf{C}$	=	cross-spectral density matrix
c_a, p_a, ρ_a	=	ambient speed of sound, pressure, and density
E	=	error function
f	=	acoustic frequency
f_c	=	one-third-octave band central frequency
H	=	Bessel function of third kind (Hankel function, $H = J + iY$)
i	=	imaginary unit
$\mathbf{k}$	=	acoustic wave vector ($\mathbf{k} = k\mathbf{u}$)
k	=	acoustic wavenumber ($k = \omega/c_a$)
J	=	Bessel function of first kind
M	=	series truncation azimuthal mode order
m	=	azimuthal mode order
N_f	=	number of frequencies in a band
N_{PW}	=	number of impinging plane waves
N_{mic}	=	number of microphones
P	=	acoustic pressure due to all plane waves
P_0	=	complex amplitude of the incident wave pressure
p	=	acoustic pressure
p^s	=	scattered acoustic pressure
p_m	=	azimuthal Fourier component of order m
R	=	beam-forming source function
R_{nl}	=	complex amplitude of the cross-spectral density between two plane waves
r_c	=	cylinder radius
$\mathbf{u}$	=	front plane wave unit vector
$\mathbf{w}$	=	beam-forming weight vector
x_1, r, φ	=	cylindrical coordinates ($r = \sqrt{x_2^2 + x_3^2}$)
(y, z)	=	source map projection plane
Y	=	Bessel function of second kind
δ_{ij}	=	Kronecker delta
ϑ_w, φ_w	=	plane wave spherical angles
ω	=	angular frequency

Superscripts

†	=	transpose complex conjugate
⋆	=	complex conjugate

I. Introduction

THE liftoff phase of a launch vehicle is characterized by severe overpressure and acoustic loads that can damage both the launcher and the payload electronic systems. The overpressure loads are due to the impingement of a blast wave generated during the engine ignition phase. This phenomenon has an impulsive transient character and is usually modeled in the time domain, as done for instance by Pavish and Deese [1]. The acoustic loads are due to the shock/turbulence mechanisms taking place in the jet plume, mechanisms that are dramatically enhanced by the interaction of the plume with the launch pad [2]. These phenomena have a broadband character and are usually modeled in the frequency domain. The present work is focused on the acoustic loads for which a frequency-domain analysis is undertaken.

The accurate determination of the acoustic levels inside the fairing of a launch vehicle is an important requirement for the dimensioning of the acoustic protection systems for the embedded electronic components. Numerical vibroacoustic analyses are undertaken to determine the internal acoustic levels, starting from a model of the external acoustic environment. This model consists of both auto and cross-spectra information. The acoustic autospectra can be estimated through measurements carried out on the surface of a scale mock-up

Presented at the 17th AIAA/CEAS Aeroacoustics Conference, Portland (OR), 5–8 June 2011; received 5 July 2011; revision received 3 December 2011; accepted for publication 12 December 2011. Copyright © 2012 by Italian Aerospace Research Center. Published by the American Institute of Aeronautics and Astronautics, Inc., with permission. Copies of this paper may be made for personal or internal use, on condition that the copier pay the $10.00 per-copy fee to the Copyright Clearance Center, Inc., 222 Rosewood Drive, Danvers, MA 01923; include the code 0001-1452/12 and $10.00 in correspondence with the CCC.

*Senior Research Engineer, Aerodynamics and Aeroacoustics Laboratory. Member AIAA.
†Aerospace Engineering Internship Student, University of Pisa.
‡Responsible for Aerodynamics and Aeroacoustics, Mechanical Subsystem Group.
§Product Engineer, Mechanical Design Group, Space Division.

Downloaded by UNIVERSITY OF TENNESSEE on March 18, 2013 | http://arc.aiaa.org | DOI: 10.2514/1.J051479

or on the real launcher during its operation. In addition, empirical models, properly calibrated through specific experimental data, can be used with a certain confidence level. The first empirical model has been developed by Eldred at NASA [3] during the 1970s, and successively modified by several authors [4,5]. The main drawback of an empirical model, regarding the determination of the noise autospectra, is that it does not take into account the wave reflections on the launcher and the real pad, and therefore specific corrections are required to predict the surface acoustic loads with an adequate accuracy. The reliability of an empirical model can be increased by taking into account the sound reflection mechanisms in the radiation part of the model. A hybrid empirical/numerical model has been for instance proposed by Casalino et al. [6] that consists in convoluting the Eldred's empirical source distribution through numerical Green's function of the whole radiation problem involving both the launcher and the pad.

The determination of the noise cross-spectra is a much more difficult task, since it requires a model of the space/time correlation of the nonlinear random phenomena occurring in the rocket plume, and of the linear acoustic phenomena occurring in the propagation field. Because of the past and present limitations of computational fluid dynamics (CFD) and computational aeroacoustics (CAA) techniques to simulate the noise generation mechanisms occurring in a rocket plume impinging on a launch pad, at a realistic scale, and taking into account the flow/geometry complexities, two alternative approaches have been developed in the past years and are currently used for launch vehicle vibroacoustics. The first one consists in using a diffuse random acoustic field, thus skipping any link with the effective noise generation and propagation mechanisms. The second approach consists in using an inverse acoustic method that, starting from the noise signals measured at some locations on the surface of the launcher, is capable to determine an equivalent source distribution and therefore to reconstruct the acoustic environment around the launcher, both in terms of auto- and cross-spectra. The main drawback of an inverse method is the necessity of a sufficient number of noise measurements on the launcher surface to increase the robustness of the method in predicting the noise spectra at locations that are far from the measurement points, up to a prescribed frequency. The robustness of an inverse method can be increased by taking into account the wave reflection on the launcher. This aspect is addressed in this work in which a beam-forming technique is proposed that makes use of elementary acoustic solutions generated by plane waves impinging on the launcher. The use of a wave propagation model to account for the real launcher geometry is not new, having been used for instance by Alestra et al. [7] who developed an acoustic inverse model in the time domain based on an optimal control method. Furthermore, the idea of modeling the acoustic field about a launcher by superposition of impinging plane waves scattered by the launcher has been already proposed by Morshed [8], who employed both analytical solutions for an infinite cylinder and boundary element method (BEM) solutions for the real launcher. A similar approach is employed in this work, with the difference that finite element method (FEM) solutions are employed.

The use of phased array measurements for noise source localization is an established practise in the beam-forming domain. Conventional beam-forming (CB) source maps are generated by convoluting the noise sources with the array response to an elementary source (usually a Dirac source), the so-called point spread function (PSF). As a consequence, maps are contaminated by a virtual spreading of the real sources (main lobes) and by the appearance of side lobes around the real sources. Deconvolution methods have been proposed in past years that consists in identifying the PSFs in a source map and replacing them by beams of narrow width. Among other methods, the CLEAN algorithm and its variants [9,10], the spectral estimation method (SEM) [11], and the DAMAS algorithm and its variants [12] have been successfully used in the aeroacoustic domain. In particular, variants of the CLEAN and DAMAS methods have been recently used by Panda and Mosher [13] to investigate the noise sources in a supersonic rocket plume; both methods have been shown to reduce the smearing associated with the PSF, but did not improve the resolution beyond the Rayleigh criterion. The inverse acoustic model presented in this study is very similar to the SEM, with the only differences that the microphones are installed on the surface of a reflecting body, the launcher mock-up, and the elementary source fields are plane waves impinging on the launcher instead of Dirac sources in freefield.

The approach presented in this paper is applied to analyze noise data acquired on a scale mock-up of the Vega launch vehicle. To this goal, measurements performed in the AVIO BEAT test facility [14] in the framework of the Italian Space Agency funded project CAST have been used. Vega is the European small launch vehicle under development by the prime contractor European Launch Vehicle S.p.A. (ELV), under the responsibility of the European Space Agency. It is constituted of four stages, and it is targeted to the scientific/commercial market of small satellites (300–2500 kg) into low Earth orbits, with inclinations ranging from 5.2 deg up to sun-synchronous orbits and with altitudes ranging from 300 to 1500 km. The first-stage motor is the P80, a carbon-epoxy filament wound monolithic motor case produced by EUROPROPULSION, a joint venture between Avio and SNECMA.

The layout of the paper is as follows. In Sec. II the methods employed to compute the launcher-tailored steering vector required by the beam-forming analysis are presented. A description of the experimental activity carried out by ELV/AVIO to measure the noise signals at different locations upon a $1/20$ scale mock-up of the Vega launcher is presented in Sec. III. In Sec. IVa CB algorithm and a deconvolution method are reviewed and source localization results are presented in Sec. V for two values of the launcher altitudes above the pad. The deconvolution method is validated in Sec. VI by using all but one of the measured noise signals to compute the equivalent noise sources, and then comparing the predicted noise spectra at the omitted microphone with the measured spectra. Finally, the main outcomes of the present work and future directions of investigation are drawn in Sec. VII.

II. Launcher Acoustic Model

The methods employed to compute the elementary acoustic fields about the Vega launcher are presented in this section. After an overview of the approach, the analytical and the numerical methods are described in Secs. II.B and II.C, respectively. The numerical model is verified in Sec. II.D against the analytical solution of a plane wave scattered by an infinite cylinder. Finally, the potential benefits associated with the use of a numerical scattering model of the real launcher instead of an analytical model of a cylinder are investigated in Sec. II.E.

A. Overview of the Model

The main idea exploited in this work is that the noise sources, both the real ones in the rocket plume and the virtual ones due to the wave reflections by the several structures around the launcher, are distributed in the whole space and their acoustic effect can be represented by plane waves impinging on the launcher from different directions. To better explain this concept, let us consider the elementary acoustic fields in Fig. 1, generated by Dirac sources in a 2-D domain in the presence of all the geometrical details of the launch

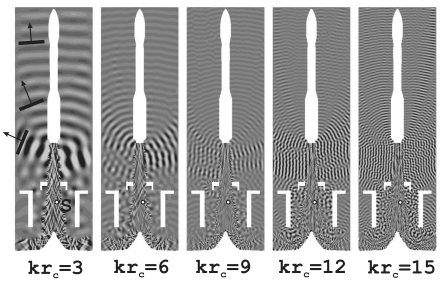

Fig. 1 FEM solutions obtained by locating a Dirac source in the plume of the Vega launcher, providing an illustration of the concept of representing the acoustic field around the fairing as a superposition of plane waves.

Downloaded by UNIVERSITY OF TENNESSEE on March 18, 2013 | http://arc.aiaa.org | DOI: 10.2514/1.J051479

pad and a realistic flow in the rocket plume. Figures show contour plots of the instantaneous acoustic pressure computed using the FEM software *Opty∂B* [15,16] for different values of the Helmholtz number kr_c, based on the P80 external radius, and for a given source location indicated with "S" in the left figure. It is interesting to observe that the wave pattern is very complex in the cove region of the launch pad, both due to the multiple reflections on the walls and diffractions at the corners, and to the wave refraction in the supersonic plume (a fully expanded flow condition has been used to compute the time-averaged flow). However, outside the cove region and in particular close to the launcher fairing, the acoustic field achieves a more regular pattern and the wave fronts can be locally approximated by plane waves. Therefore, it becomes natural to focus only on the acoustic field close to the fairing and modeling it as a superposition of plane waves.

In the present approach, each plane wave is decomposed into a Fourier series of axial-symmetric components, each one for an azimuthal order; the whole 3-D solution is then reconstructed by inverse Fourier series. The problem of plane wave scattered by an infinite cylinder can be solved analytically by means of the same azimuthal wave decomposition. Therefore, it becomes natural to use these analytical solutions to verify the numerical approach for the case of a cylinder. Moreover, the analytical solutions for a cylinder of radius equal to the launcher radius at the microphone axial location can be used as an alternative to the numerical solutions tailored to the real launcher geometry, thus resulting in faster beam-forming analyses.

The present analysis covers the range 20–284 Hz (full-scale), with a frequency step of 4 Hz, corresponding to a full coverage of the one-third-octave central frequency range 25–250 Hz. In terms of Helmholtz number based on the P80 external radius, the analysis range is 0.55–7.87. The use of a 2-D numerical model results in affordable computational times: about 30 h on a single processor laptop.

B. Analytical Acoustic Model

In this subsection the analytical solution of plane waves impinging on an infinite cylinder is presented. Although similar analytical formulas can be found in the literature [17], it is useful to provide the expressions used in this work with reference to the conceptual scheme and reference system illustrated in Fig. 2.

A launch vehicle is a body with axial symmetry. To compute analytically the acoustic field due to an impinging plane wave with wave vector **k**, it can be supposed that the acoustic field in the neighborhood of the microphone located for instance on the fairing of the launcher, as shown in Fig. 2, can be estimated by locally approximating the launcher by an infinite cylinder of radius equal to the launcher radius at the axial location of the microphone. The impinging plane waves are distributed in the whole 3-D domain and reproduce the effect due to real sources in the rocket plume and waves reflected by the several structural elements that are present in the launch pad. The direction **u** of the wave vector **k** is defined by two angles, i.e., ϑ, varying in the interval $[-\pi: 0]$, and φ, varying in the interval $[0: 2\pi]$. The generic impinging plane wave of magnitude P_0 has the expression $p = P_0 \exp(i\mathbf{k}\cdot\mathbf{x})$ ($-i\omega t$ convention). The modulus of the wave vector is $k = \omega/c_a$. The Cartesian components of the unit wave vector are: $u_1 = \cos\vartheta_w$, $u_2 = \sin\vartheta_w \cos\varphi_w$, and $u_3 = \sin\vartheta_w \sin\varphi_w$.

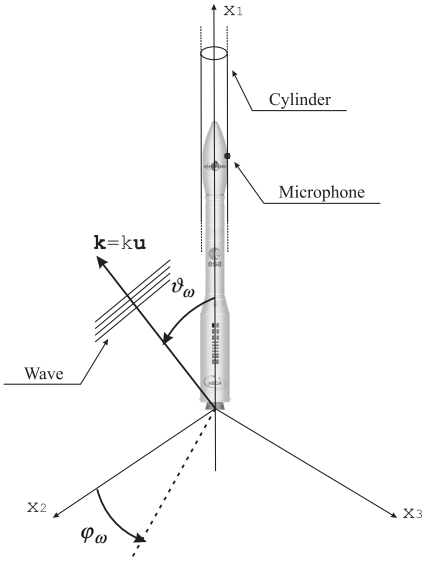

Fig. 2 Illustration of the conceptual scheme of a plane wave impinging on a launcher, and its local modeling as an infinite cylinder.

The analytical expression of the acoustic pressure field can be obtained, as shown for instance by Morse and Ingard [18], by decomposing the incident plane wave into a series of axial-symmetric modes of azimuthal order m. Denoting as $p_m(x_1, r)$ the axial-symmetric solution for the azimuthal order m, the 3-D acoustic field is obtained by the following series summation truncated at the order M:

$$p(x_1, r, \varphi) = \frac{p_0(x_1, r)}{2\pi} + \frac{1}{\pi}\sum_{m=1}^{M} p_m(x_1, r)\cos(m\varphi) \tag{1}$$

This formula has a general validity and can be used, for instance, to compute a 3-D Green's function as a superposition of Dirac-ring solutions, as shown in [15,16]. The impinging plane wave azimuthal decomposition that is compatible with the above reconstruction is:

$$p_m(x_1, r) = 2\pi J_m(-k_2 r)(-i)^m e^{ik_1 x_1}, \quad \text{with} \quad m = 0 \ldots M \tag{2}$$

where J_m is the m-th order Bessel function and $k_2 (\leq 0)$ is the wavenumber in the radial direction. The plane wave scattered pressure has the following expression in cylindrical coordinates:

$$p^s(k; x_1 r, \varphi; \vartheta_w, \varphi_w) = e^{ik_1 x_1}\left\{A_0 H_0(-kr\sin\vartheta_w) + \sum_{m=1}^{M} A_m \cos[m(\varphi - \varphi_w)] H_m(-kr\sin\vartheta_w)\right\} \tag{3}$$

where ϑ_w and φ_w are the angular directions of the plane wave, $r = \sqrt{x_2^2 + x_3^2}$, and H_m denotes the Hankel function of order m. The coefficients A_m of the series expansion are given by:

$$A_m = -\epsilon_m P_0 i^{m+1} e^{-i\gamma_m}\sin(\gamma_m), \quad \text{with} \quad m = 0 \ldots M \tag{4}$$

where $\epsilon_0 = 1$, $\epsilon_m = 2$ ($m \neq 0$) and the angle γ_m is such that:

$$\tan(\gamma_0) = -\frac{J_1(-kr\sin\vartheta_w)}{Y_1(-kr\sin\vartheta_w)}$$
$$\tan(\gamma_m) = -\frac{J_{m+1}(-kr\sin\vartheta_w) - J_{m-1}(-kr\sin\vartheta_w)}{Y_{m+1}(-kr\sin\vartheta_w) - Y_{m-1}(-kr\sin\vartheta_w)} \tag{5}$$

C. Numerical Acoustic Model

The numerical computation of plane waves scattered by the launcher is conducted by using the FEM code *Opty∂B*, recently developed by Casalino [15,16] to solve a wide class of acoustic and aeroacoustic problems [19–21]. For the sake of the present work, the Helmholtz equation is solved, since a wave propagation in a quiescent fluid is addressed. The code exploits a continuous Galerkin discretization based on the Astley and Eversman [22] frequency-domain formulation. The Helmholtz equation is solved for each azimuthal component of the plane wave in axial-symmetric modality. One of the key aspects of the present FEM code is the management of the boundary conditions. These are applied by adding to the unknowns vector the normal derivatives of the acoustic variables at all the boundary nodes. The boundary condition matrix is computed separately from the field matrix, the overall linear system is assembled for a specific value of k, and finally solved using a direct solver. If parametric conditions are imposed on one or more than one

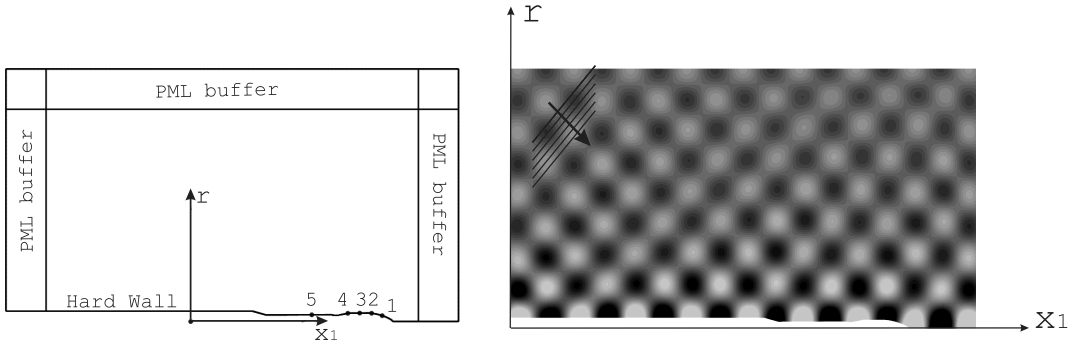

Fig. 3 FEM computational domain and boundary conditions on the left and an example of FEM solution on the right. Microphones at five axial locations are plotted as bullets on the launcher fairing.

boundaries, then the linear system is solved for all the resulting right-hand sides. This is the case of the different plane waves injected into the computational domain. Several and flexible boundary conditions are available in the code and permit to address a variety of practical problems. For the present simulations, hard-wall boundary conditions are prescribed on the surface of the space launcher, whereas a perfectly matched layer (PML) approach is used to force the plane waves on the radiation boundaries and to damp the outgoing waves reflected by the launcher. Figure 3 shows the computational domain, the boundary conditions, the microphone axial locations where the numerical elementary solutions are extracted for the beam-forming model, and an example of solutions obtained for the azimuthal number $m = 0$, frequency $f = 56$ Hz, and a plane wave with direction $\vartheta_w = -45$ deg and $\varphi_w = 0$ deg. The computational domain extends from -27.6 to 40 m in the axial direction, and from 0 to 37.6 m in the radial direction. It is discretized with $352 \cdot 10^3$ number of nodes and $703 \cdot 10^3$ number of triangular elements, corresponding to about 10 points per acoustic wavelength at the maximum analysis frequency of 284 Hz. The computational domain has been virtually extended in the negative axial direction and the basis of the launcher corresponds to $x_1 = 0$.

FEM computations are carried out in the plane (x_1, x_2) by considering only plane waves with direction $\varphi_w = 0$. The solutions at microphones located at nonzero azimuthal angles φ are reconstructed in a postprocessing phase through a series summation over the whole set of axial-symmetric solutions. The solution at the generic azimuthal angle φ_m for a plane wave impinging from the generic direction φ_w is equal to the solution reconstructed at the angle $\varphi_m - \varphi_w$.

Equation (2) providing the azimuthal component of a plane wave is used to compute the forcing term of the FEM model, i.e., the right-hand side of the wave equation solved in all the PML buffers, as described for instance by Casalino [15].

D. Verification of the Numerical Wave Scattering Model

To verify the numerical technique employed in this work to compute the 3-D acoustic field due to a plane wave impinging on a launch vehicle, the scattering from a cylinder with a finite axial extension is computed and compared with the analytical solution for an infinite cylinder.

A cylinder of unitary radius r_c and axial extension equal to 20 is considered. The 2-D mesh extends from 0 to 20 in the axial direction and from 1 to 11 in the radial direction. The rectangular computational domain is discretized with a Cartesian mesh consisting of 100 and 51 points in the axial and radial directions, respectively. Two Helmholtz numbers are considered: $kr_c = 1.5637$ ($f = 85$ Hz) and $kr_c = 3.1273$ ($f = 170$ Hz). The plane wave angle is $\theta_w = -42.35$ deg. The 3-D solutions are computed by summation over 21 axial-symmetric solutions ($M = 20$). The ambient conditions are $p_a = 101325$ Pa and $\rho_a = 1.216$ kg/m^3.

Figure 4 shows the comparison between analytical and FEM solutions for the frequencies $f = 85$ and 170 Hz. A good agreement is obtained although the numerical solution is computed for a

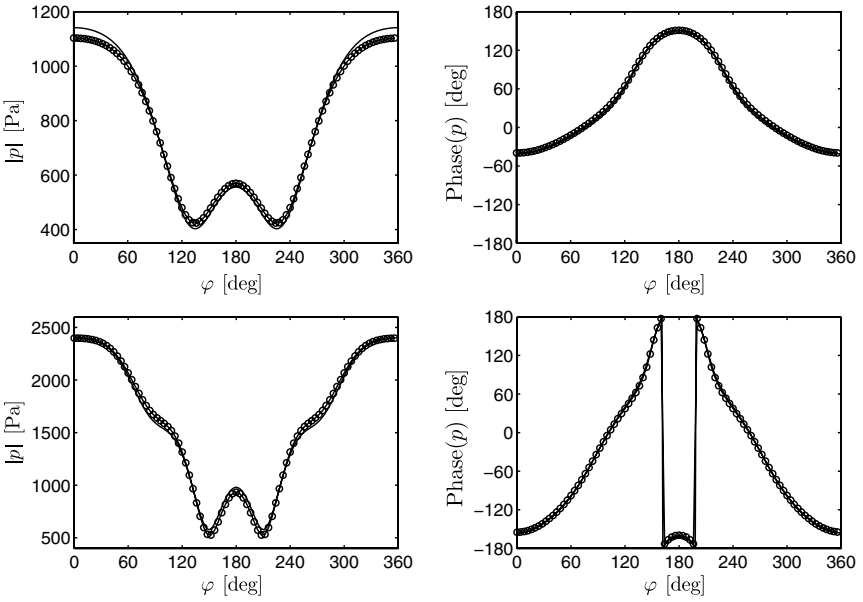

Fig. 4 Plane-wave scattering from a cylinder of radius r_c. Comparison between numerical (lines) and analytical (symbols) acoustic pressure solutions along the cylinder surface at the mid axial section. Modulus on the left, phase on the right. Helmholtz number $kr_c = 1.5637$ on the top and $kr_c = 3.1273$ on the bottom.

Downloaded by UNIVERSITY OF TENNESSEE on March 18, 2013 | http://arc.aiaa.org | DOI: 10.2514/1.J051479

cylinder of finite axial extent. At $f = 85$ Hz, the L_2 relative discrepancies are 2.75 and 3.09% for the modulus and phase, respectively; whereas the same quantities at $f = 170$ Hz are 2.27 and 1.74%. The slightly better agreement between numerical and analytical solutions at the higher frequency is due to the fact that, in this case, the numerical solution attains a better representation of an infinite cylinder, since the ratio between the acoustic wavelength and the axial extent of the cylinder is higher.

E. Influence of Geometry on the Acoustic Wall Pressure Levels

To investigate the potential benefits associated with a more accurate scattering model, the analytical and numerical solutions along the first microphone ring of Fig. 3 ($r_c = 0.87$ m) are computed for the frequencies 20 and 250 Hz and compared in terms of sound pressure level (SPL). Results obtained considering two values of the wave impinging angle ϑ_w are plotted in Fig. 5. The two solutions are in a 1 dB agreement at low frequency, but differences up to 5 dB occur for the high-frequency case. According to these results, the influence of the real geometry on the prediction of the wall pressure acoustic levels cannot be a priori neglected in the frequency range addressed in the present work.

III. Vega Scale Mock-Up Firing Tests

Experiments consisting in a number of firings of a 1/20 scale mock-up of the Vega launcher have been conducted by ELV/AVIO with the support of Centro Italiano Ricerche Aerospaziali (CIRA) in the Banco Esperimenti AcusTici (BEAT) facility located in Colleferro, Italy, described by Mascanzoni and Contini [23]. This activity has been funded by the Italian Space Agency through the national research project CAST coordinated by CIRA.

As shown in the pictures of Fig. 7, the mock-up is suspended through a vertical strut at different altitudes above the launch pad that is a scale model of the ELA-1 launch pad (now Vega-Pad) of the European Space Center in French Guiana. The geometry of the launch pad and the profile of the plume deflector are also shown in the same figure.

The design of the BEAT facility, and in particular of the launcher mock-up, was conceived to reproduce the same acoustic environment generated by the full-scale Vega first-stage solid rocket motor (SRM) P80 at different launcher altitudes, from 0 to 75 m, corresponding to the first 4 s of Vega ascent trajectory during liftoff. The P80 simulator operates in the same pressure chamber and nozzle expansion ratio conditions of the full-scale rocket motor; thus, it generates a jet plume that is characterized by the same Strouhal number, velocity, pressure, density, and temperature as the full-scale jet. The P80 SRM has an external diameter of about 3 m and a nozzle diameter of about 2 m. The full length of the Vega launcher is about 31 m.

Three scaled altitudes have been considered during the experiments: 0, 0.5, and 3.75 m. A number of flush mounted microphones are located on the surface of the mock-up. The present beam-forming analysis makes use of 15 microphones located, as shown in Fig. 6, at different azimuthal angles along three of the five axial locations indicated in Fig. 3.

Figure 7 shows clearly the presence of different structural elements around the mock-up that are responsible for multiple wave reflections that are expected to be captured by the beam-forming algorithm.

The noise acquisition system consists of flush mounted "pressure-type" microphones and preamplifiers, a data acquisition system (DAS) for the acoustic measurements, a ballistic acquisition system (BAS) for engine performance measurements, and an environmental unit for the measurement of air temperature, humidity, and wind velocity. The acoustic and ballistic sensor output are filtered by a signal conditioning system (SCS) before they are acquired. A schematic representation of the different systems is shown in Fig. 8. Microphones of model PCB 377A10 are used (size: 1/4 in., sensitivity: 1.6 mV/Pa, dynamic range: 170 dB, frequency range: 4 Hz–70 kHz). Preamplifiers with prepolarized capsule of model PCB 426B03 are used (size: 1/4 in., frequency range: 5 Hz–126 kHz). The DAS and SCS are composed of one data acquisition system National Instruments with a capacity of 64 channels at 100 kHz, one magnetic recorder Sony SIR 1000 with a capacity of 16 channels at 96 kHz each, and five cabinets of signal conditioner, model PCB 481A, with a capacity of 16 channels each. The evaluation of the P80 simulator engine performances during the acoustic tests is accomplished using a dedicated BAS, which detects the pressure levels measured in the engine combustion chamber through a pressure transducer up to $90 \cdot 10^5$ Pa. The acquisition of

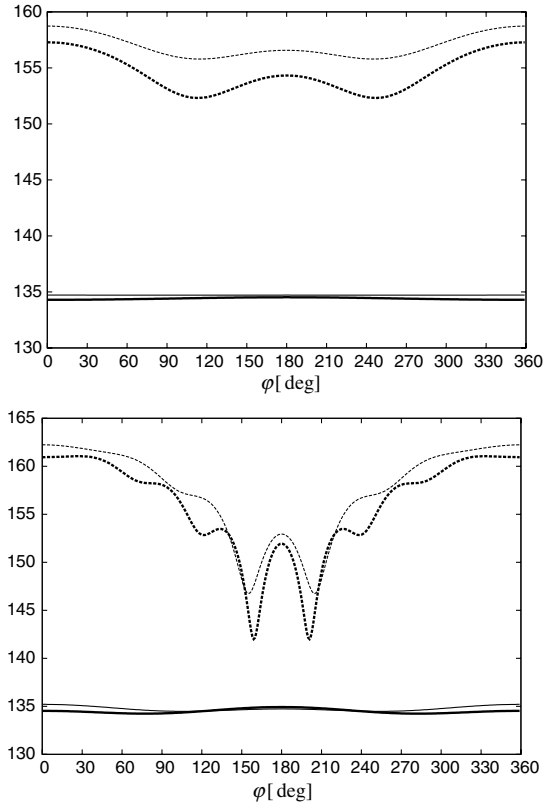

Fig. 5 SPL [dB, $p_{ref} = 2 \cdot 10^{-5}$] along the first microphone ring of Fig. 3 computed for $\vartheta_w = -6$ deg (top) and $\vartheta_w = -42$ deg (bottom). Comparison between cylinder (thin lines) and launcher (thick lines) results for three values of the acoustic frequency: $f = 20$ Hz (——) and $f = 250$ Hz (----).

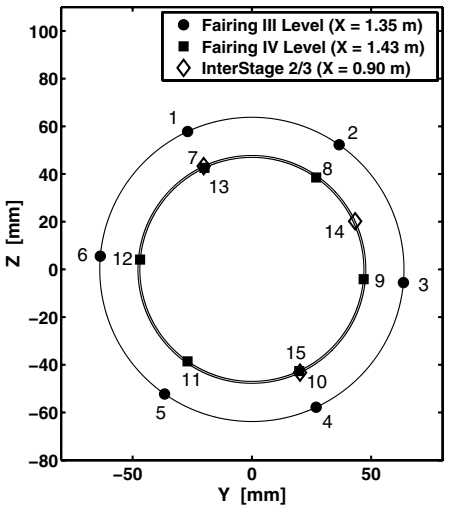

Fig. 6 Microphone distribution on Vega mock-up. Microphones 1–6 located along the ring 2 of Fig. 3, microphones 7–12 along the ring 1 and microphones 13–15 along the ring 5.

Downloaded by UNIVERSITY OF TENNESSEE on March 18, 2013 | http://arc.aiaa.org | DOI: 10.2514/1.J051479

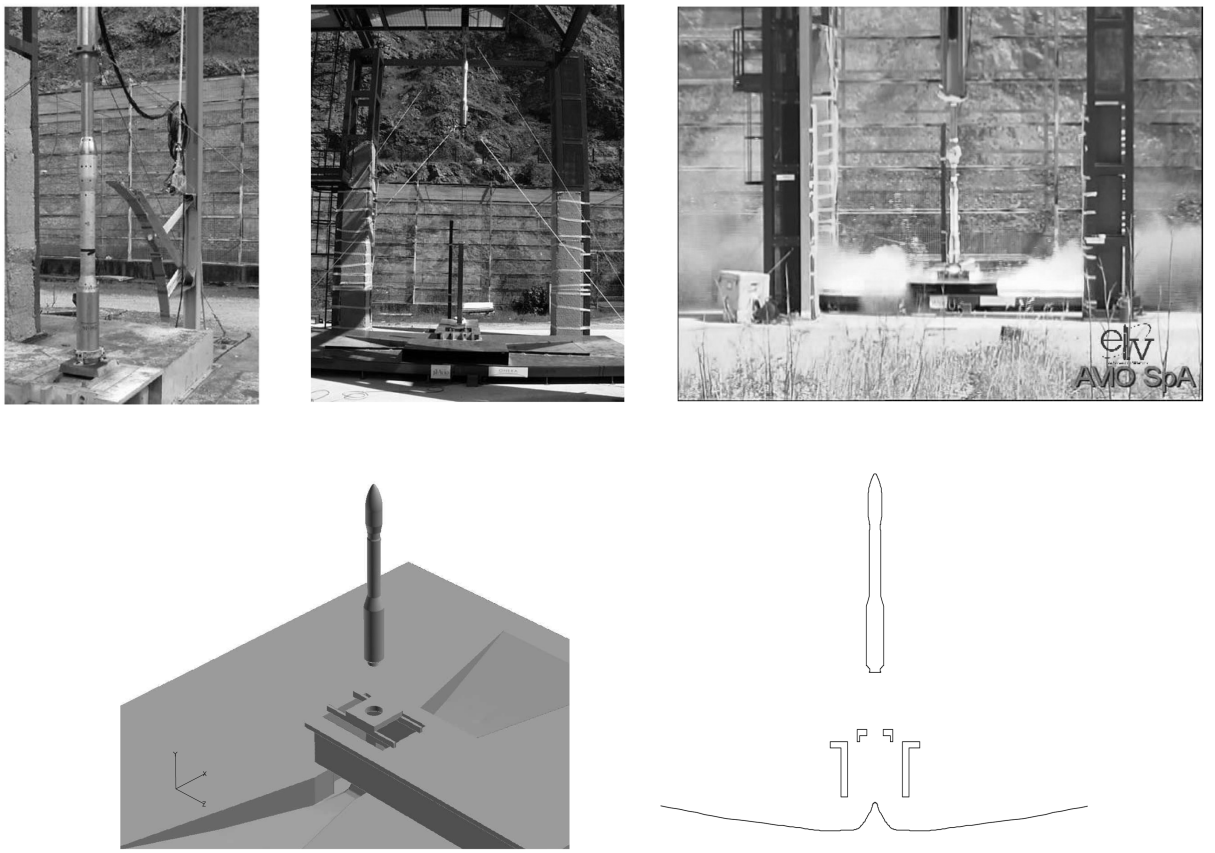

Fig. 7 On the top, pictures of the AVIO BEAT facility and Vega scale mock-up; on the bottom, numerical model of the launch pad and plume deflector, as in [6].

Downloaded by UNIVERSITY OF TENNESSEE on March 18, 2013 | http://arc.aiaa.org | DOI: 10.2514/1.J051479

the chamber pressure levels is synchronized with the acquisition of the wall pressure fluctuations measured by the microphones.

Noise signals are sampled with a rate of 104167 Hz. A number of 2^{20} samples are stored for each microphone, covering a time duration of 10 s. In addition to the noise signals, the pressure inside the rocket chamber is measured and it is used during the data analysis stage to define a suitable interval of statistically permanent conditions. The burning transitory, in fact, is characterized by an impulsive overpressure that is due to the ignition process and to the presence of internal valves that stabilize the rocket flame, followed by a quasi-permanent stage of few seconds, during which the combustion process attains a stabilized condition before the solid propellent is completely burnt.

IV. Beam-Forming Algorithms

The wall pressure fluctuations on the launcher surface can be supposed to be originated by acoustic plane waves impinging on the launcher from a multitude of directions. The elementary field $p(\omega, \mathbf{u}, \mathbf{x})$ due to a generic incident plane wave of unitary magnitude and the resulting scattered wave can be computed analytically using the formula presented in Sec. II.B or numerically through the method outlined in Sec. II.C. Therefore, two sets of basis functions are available for the beam-forming analysis.

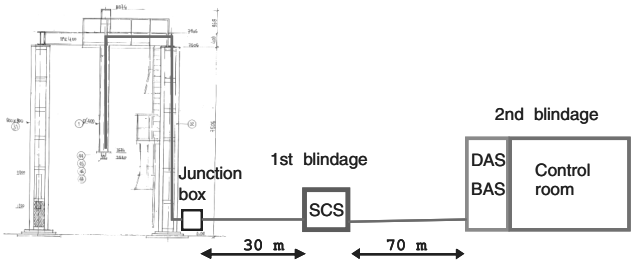

Fig. 8 Schematic illustration of the BEAT acquisition system.

A. CB Formulation

The CB is a well-established frequency-domain method allowing to determine an equivalent source distribution that, in the present case, represents the amplitude of the impinging plane waves. During the experiments, noise signals are acquired at $N_{\text{mic}} = 15$ microphones (see Fig. 6). Let us denote as $\mathbf{x}_j$ the location of the jth microphone and $\mathbf{C}$ the measured $N \times N$ cross-spectral density matrix (CSDM). Then, let $\mathbf{p} \equiv p(\omega, \mathbf{u}, \mathbf{x}_j)$ be the N-dimensional steering vector, which consists of complex pressure amplitudes induced by a unit plane wave with angular frequency ω and direction $\mathbf{u}$. If S is a subset of all possible (i, j)-combinations where i and j are microphone indices, then the value of $R(\omega, \mathbf{u})$ can be obtained through the following expression:

$$R(\omega, \mathbf{u}) = \sum_{(i,j)\in S} p_i^* C_{ij} p_j \Big/ \sum_{(i,j)\in S} |p_i|^2 |p_j|^2 \tag{6}$$

To remove the microphone self-noise contamination, the diagonal is usually removed from the CSDM. Hence, introducing the trimmed CSDM $\bar{C}_{ij} = C_{ij}(1 - \delta_{ij})$, where δ_{ij} is the Kronecker delta, and the weight vector $\mathbf{w}$:

$$\mathbf{w} = \mathbf{p} \Big/ \left(\sum_{(i,j)\in S} |p_i|^2 |p_j|^2 \right)^{1/2} \tag{7}$$

we can write the following CB compact formula:

$$R = \mathbf{w}^\dagger \bar{\mathbf{C}} \mathbf{w} \tag{8}$$

The frequency range of validity of the beam-forming results depends on the geometrical characteristics of the microphone array:

the maximum frequency is related to the minimum distance between two adjacent microphones (spatial aliasing), while the minimum frequency is related to the aperture of the array (Rayleigh criterion). The frequency range associated with the 15 microphones on the Vega mock-up is estimated to be 25–250 Hz (full-scale). The analyses are conducted in the range 20–284 Hz to cover the one-third-octave bands centered at 25 and 250 Hz.

It can be reasonably supposed that, in the case of a broadband noise generation process like the one associated with the plume of a rocket plume, the function $R(\omega, \mathbf{u})$ is a continuous and smooth function of the frequency, i.e., the localization of the noise sources varies slowly with frequency. Under this assumption, to reduce the number of source maps, it is possible and convenient to average the spectral quantities in Eq. (8) in one-third-octave bands, i.e.

$$\bar{R}(f_c, \mathbf{u}) = \frac{1}{N_f} \sum_{f \in B(f_c)} (\mathbf{w}^\dagger \bar{\mathbf{C}} \mathbf{w}) \tag{9}$$

where $B(f_c)$ represents the band centered at the frequency f_c and N_f is the number of frequencies within the band $B(f_c)$ at which $\bar{\mathbf{C}}$ is evaluated. In this work band-averaged source maps $\bar{R}$ are computed, but the steering vector and the cross-spectral matrix are evaluated with a constant frequency spacing of $\Delta f = 4$ Hz. In this case, the only advantage of using Eq. (9) is to reduce the number of source maps to be generated, plotted and analyzed. The function $\bar{R}(f_c, \mathbf{u})$ is computed by considering 870 plane wave directions $\mathbf{u}$, 29 along ϑ (from −174 to −6 deg every 6 deg) and 30 along φ (from 0 to 348 deg every 12 deg).

B. Source Localization Maps

For the scope of a space launcher noise source identification, it is convenient to represent the spherical source localization maps (plane wave directions uniformly distributed in the whole 3-D space) on the launcher basis plane (y, z). This is accomplished by using the following topological transformation:

1) For $-\pi/2 < \vartheta \leq 0$ (ground sources)

$$y = \sqrt{2}\sin(\vartheta/2)\cos\varphi$$
$$z = \sqrt{2}\sin(\vartheta/2)\sin\varphi$$

2) For $-\pi \leq \vartheta \leq -\pi/2$ (sky sources)

$$y = -\sqrt{2}\sin((\pi + \vartheta)/2)\cos\varphi$$
$$z = -\sqrt{2}\sin((\pi + \vartheta)/2)\sin\varphi$$

This transformation has the property of preserving the solid angle, i.e., $\mathrm{d}\Omega = \sin\vartheta\,\mathrm{d}\vartheta\,\mathrm{d}\varphi = \mathrm{d}y\,\mathrm{d}z$. In the plane (y, z) a circumference of radius $r = -\sqrt{2}\sin(\vartheta/2)$ represents all the plane waves from the angular direction ϑ. For each central frequency f_c, two circular maps of unitary external radius and representing the source from the ground and from the sky are therefore generated and represented. During the liftoff of a space launcher it can be reasonably expected that most of the source radiation comes from the ground semisphere, since noise is generated by the jet plume impinging on the pad. In the specific case of the Vega launcher, the ground source maps should reproduce the presence of two opposite exhaust evacuation ducts. However, due to the presence of several struts around the launcher, both on the real launch pad and the test bench, reflected indirect waves are expected to impinge on the launcher also from the sky semisphere. It is therefore useful to analyze both the ground and the sky source maps.

C. Acoustic Deconvolution Formulation

As pointed out in the introductive section, a crucial aspect of a fairing vibroacoustic analysis is the accurate modeling of the external acoustic field, both in terms of auto- and cross-spectra. In this work, an inverse method based on scale mock-up measurements is used to circumvent any analysis involving the noise generation, diffraction and refraction mechanisms occurring in proximity of the launch pad. More precisely, a deconvolution algorithm is used to determine an equivalent distribution of complex plane wave amplitudes. These can be finally used to convolute elementary acoustic fields and thus determine the noise cross-spectra on the launcher surface.

The main difficulty in deriving an acoustic deconvolution formulation is related to the nonuniqueness of the equivalent source distribution. The problem is overcome by constraining the source distribution to recover the statistics of the pressure field and thus the signal energy and the mutual microphones correlations instead of reproducing the instantaneous values of the pressure fluctuations at the measurement points, or the complex value of the acoustic pressure in the frequency domain. The formulation used in this paper is very similar to the SEM technique put forward by Blacodon and Élias [11]. It is based on the minimization, at different values of the acoustic frequency, of the square norm of the difference between the CSDM computed from the measured wall pressure signals, denoted as $\mathbf{C}$, and the CSDM modeled through a combination of elementary solutions (analytical or numerical) and denoted as $\mathbf{C}^{\mathrm{mod}}$, i.e.

$$E(f) = \|\mathbf{C}(f) - \mathbf{C}^{\mathrm{mod}}(f)\|^2 \tag{10}$$

As in the CB algorithm, we suppose that the launcher is invested by a multitude of plane waves impinging from every direction of the surrounding space. Denoting as N_{PW} the total number of impinging waves, $\mathbf{u}_n$ the nth wave and $\mathbf{x}_j$ the location of the jth microphone, the frequency expression of the overall acoustic pressure P at the point $\mathbf{x}_j$ is:

$$P(\omega, \mathbf{x}_j) \equiv P_j(\omega) = \sum_{n=1}^{N_{\mathrm{PW}}} P_0(\omega, \mathbf{u}_n) p(\omega, \mathbf{u}_n, \mathbf{x}_j)$$
$$= \sum_{n=1}^{N_{\mathrm{PW}}} P_{0n}(\omega) p_{jn}(\omega) \tag{11}$$

where $P_{0n}(\omega)$ is the magnitude of the plane wave having wave vector $\mathbf{k} = k\mathbf{u}_n$, and $p_{jn}(\omega)$ is the corresponding pressure value computed through the analytical or the numerical formulation. More precisely, $P_j(\omega)$ denotes the contribution to the one-sided Fourier spectrum at the point $\mathbf{x}_j$ and frequency f due to the N_{PW} impinging waves. The generic element C_{ij}^{mod} of the modeled CSDM can be expressed as:

$$C_{ij}^{\mathrm{mod}} = P_i(\omega) P_j^*(\omega) = \sum_{n=1}^{N_{\mathrm{PW}}} \sum_{l=1}^{N_{\mathrm{PW}}} [P_{0n}(\omega) P_{0l}^*(\omega)] p_{in}(\omega) p_{jl}^*(\omega) \tag{12}$$

If N_{mic} is the number of pressure signals used for the computation of the CSDM, it is then necessary to minimize the quantity:

$$E(\omega) = \sum_{i=1}^{N_{\mathrm{mic}}} \sum_{j=1}^{N_{\mathrm{mic}}} \left| C_{ij}(\omega) - \sum_{n=1}^{N_{\mathrm{PW}}} \sum_{l=1}^{N_{\mathrm{PW}}} [P_{0n}(\omega) P_{0l}^*(\omega)] p_{in}(\omega) p_{jl}^*(\omega) \right|^2 \tag{13}$$

with respect to the amplitude P_0 of the impinging plane waves. Since the number of impinging waves is assumed to be greater than the number of microphones ($N_{\mathrm{PW}} > N_{\mathrm{mic}}$), the minimization of the above quantity leads to the solution of an underdetermined nonlinear complex system. To recover the linearity of the problem and thus apply a least-square linear system solver, it can be supposed that the plane waves are not correlated. By introducing the quantity $R_{nl}(\omega) = P_{0n}(\omega) P_{0l}^*(\omega)$ that represents the complex amplitude of the cross-spectral density between two plane waves, the hypothesis of uncorrelated waves leads to the following expression:

$$R_{nl}(\omega) = R_{nn}(\omega)\delta_{nl} \tag{14}$$

where $R_{nn} = |P_{0n}|^2$ is the PSD of the plane wave of wave vector $\mathbf{u}_n$. This yields the following expression of the linearized CSDM:

$$C_{ij}^{\mathrm{mod}} = \sum_{n=1}^{N_{\mathrm{PW}}} R_{nn}(\omega) p_{in}(\omega) p_{jn}^*(\omega) \tag{15}$$

Downloaded by UNIVERSITY OF TENNESSEE on March 18, 2013 | http://arc.aiaa.org | DOI: 10.2514/1.J051479

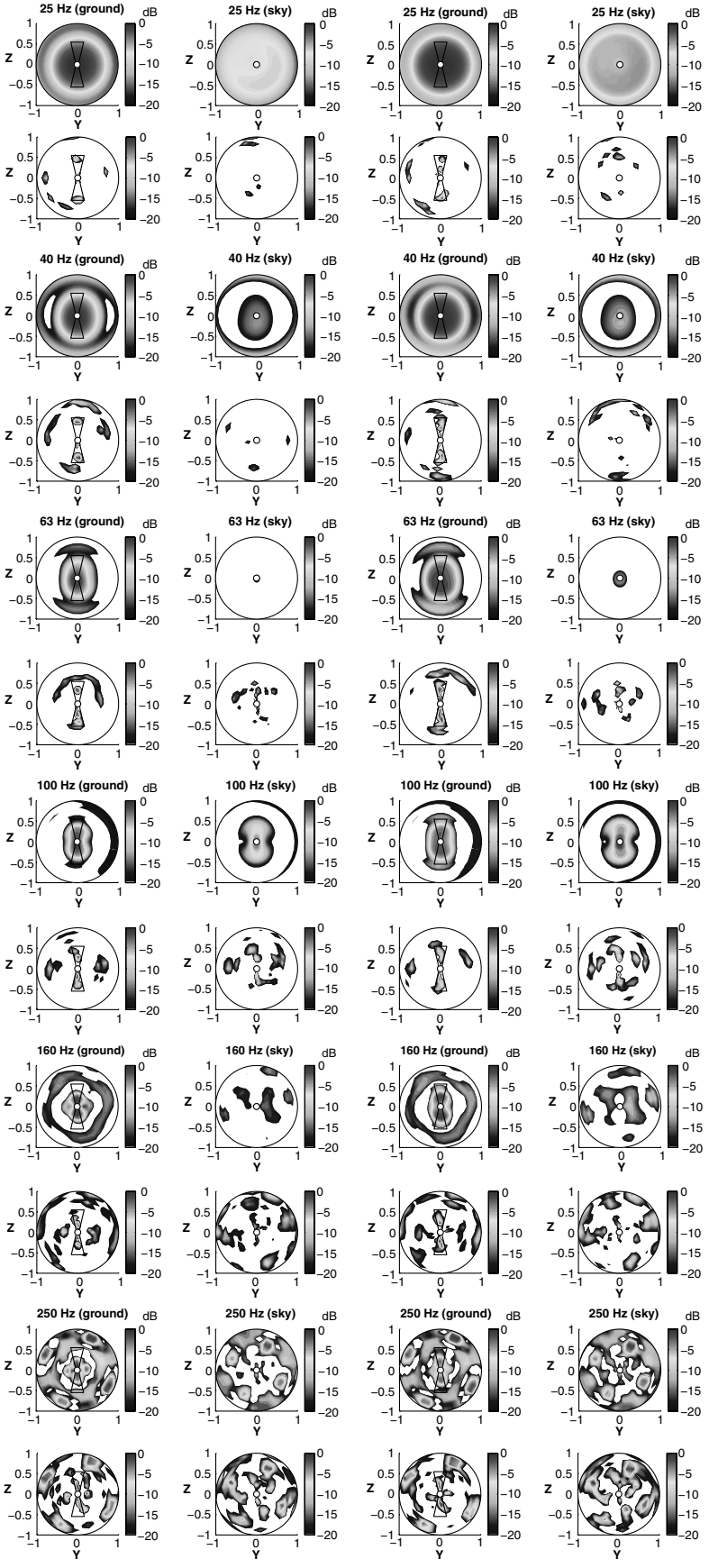

Fig. 9 CB and SEM results (alternate rows). Launcher at 0 m above the pad. Analytical plane wave results on the left and FEM results on the right.

Downloaded by UNIVERSITY OF TENNESSEE on March 18, 2013 | http://arc.aiaa.org | DOI: 10.2514/1.J051479

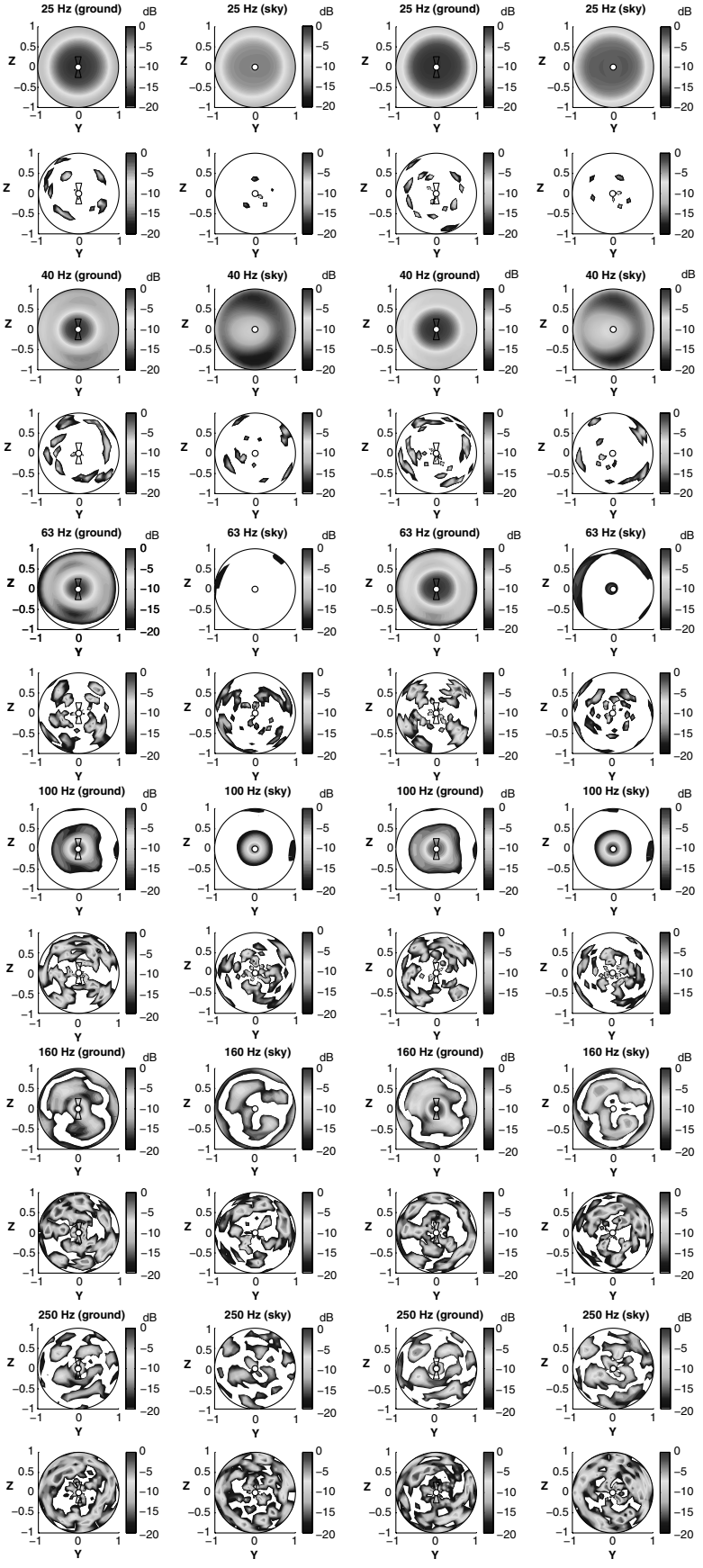

Fig. 10 CB and SEM results (alternate rows). Launcher at 75 m above the pad. Analytical plane wave results on the left and FEM results on the right.

Downloaded by UNIVERSITY OF TENNESSEE on March 18, 2013 | http://arc.aiaa.org | DOI: 10.2514/1.J051479

The minimization is therefore applied to the following quantity:

$$E(\omega) = \sum_{i=1}^{N_{\text{mic}}} \sum_{j=1}^{N_{\text{mic}}} \left| C_{ij}(\omega) - \sum_{n=1}^{N_{\text{PW}}} R_{nn}(\omega) p_{in}(\omega) p_{jn}^{*}(\omega) \right|^2 \tag{16}$$

with respect to the unknowns $R_{nn}(\omega)$ that are all real and positive. Therefore, the solution of the undetermined linear system can be carried out using the nonnegative least-square method [24] implemented in Matlab™ routine *lsqnonneg*.

The unknowns $R_{nn}(\omega)$ are computed by considering 870 plane wave directions $\mathbf{u}$, with the same discretization as for the CB source maps. The CSDM is computed through the method of the periodogram in the frequency range [20–284 Hz], with a frequency interval $\Delta f = 4$ Hz. The minimization is therefore carried out for 67 constant spaced frequency values, whereas the noise spectra reconstruction is carried out in third-octave frequency bands, by cumulating the energy contribution over each band and by considering the phase of the central frequency contribution.

V. Source Localization Results

In this section contour plots of the source function $\bar{R}$ computed using both CB and SEM techniques are presented and discussed. Following the approach described in Sec. IV.B, for each one-third-octave band central frequency in the range 25–250 Hz, both ground and sky semispheres are projected on two circular maps. Results obtained by using the analytical functional basis and the numerical one are compared with each other. Source levels are represented in dB relative to the peak value in the map.

The spectral analysis has been carried out considering the part of the measured noise signals that exhibit a statistically constant behavior. The overall duration of each signal is 201.3264 s (full-scale), sampled with a time rate of $1.92\dot{1}0^{-4}$ s. The time intervals used for the analyses is 32 s.

Two values of the launcher altitude above the pad are considered, i.e., 0 and 75 m; CB results for the altitude of 10 m can be found in [25]. The CB and SEM maps for the case $h = 0$ m are shown in Fig. 9. Interestingly, the analytical and numerical functional bases provide very similar results in the whole frequency range. This result is quite surprising since, as pointed out in Sec. II.E, the launcher geometry has a significant effect on the surface acoustic levels. In the frequency range 25–40 Hz, the CB ground sources exhibit a quite axial-symmetric pattern and seem to be concentrated around the launcher axis. This is, however, an artifact of the fair resolution of the CB technique at low frequency. In fact, the corresponding SEM maps show the presence of sources close to the terminations of the exhaust ducts. For the same reason, significant sky source levels are present in the CB map at 25 Hz, whereas only few small sources are present in the corresponding SEM map. In the frequency range 63–160 Hz, the ground sources exhibit a butterfly pattern that clearly reveals the effect of the rocket plume splitting, deflection, and flowing through the two opposite exhaust ducts of the launch pad. This effect is more evident at higher frequencies because the beam-forming resolution improves when frequency increases. The sources in the exhaust ducts are even more evident in the SEM maps. Interestingly, the sources approach the launcher axis as the frequency increases, and this effect can be explained by considering that the dominant frequency of the noise sources in the rocket plume decreases as their distance from the nozzle increases. Moreover, the jet impingement and splitting on the deflector is a source of higher frequency noise. An alignment error of few degrees of the mock-up with respect to the axes of the launch pad can be observed (rotation around x_1 axis). Finally, in the high-frequency range 160–250 Hz, both ground and sky source maps exhibit typical CB side lobes that can be reduced but not eliminated using the SEM deconvolution. Because of the presence of side lobes, it is difficult to appreciate the effect due to spurious reflections on the structural elements of the test bench.

The CB and SEM maps for the case $h = 75$ m are shown in Fig. 10. The CB maps exhibit an axial-symmetric pattern up to 100 Hz, whereas at higher frequencies these are corrupted by the side lobes. Analogously the SEM maps exhibit sources that are uniformly distributed along the azimuthal direction and no effects is evident anymore due to the presence of the exhaust ducts. Again, very similar results are obtained using the analytical and the numerical radiation models.

The results shown in this section have been computed by using 21 azimuthal modes and 15 microphones. Because of the small number of microphones compared with the azimuthal mode order, it is worthwhile to investigate the influence of the truncation order M on the CB maps. Computations have been performed for the launcher at 0 m above the pad and at a frequency of 250 Hz. Figure 11 show CB maps computed with four increasing values of M. From this source map it seems that no significant differences can be observed between $M = 5$ and $M = 10$. Further analyses will be conducted in the future to find the best trade-off between convergence of the source reconstruction algorithm and computational time.

VI. Acoustic Field Reconstruction Results

In this section results are presented that validate the capability of the acoustic deconvolution algorithm described in Sec. IV.C to reconstruct the wall pressure auto- and cross-spectra at locations where noise measurements are not available. The procedure used to produce these results consists in determining the equivalent source distribution in the different frequency bands by omitting the microphone 1 from the wall pressure CSDM. Then the pressure cross-spectra between microphone 1 and the other ones are computed and compared with the cross-spectra computed from the measured wall pressure signals.

Figure 12 shows the predicted spectra for three values of the launcher altitudes above the pad. The measured spectra are plotted

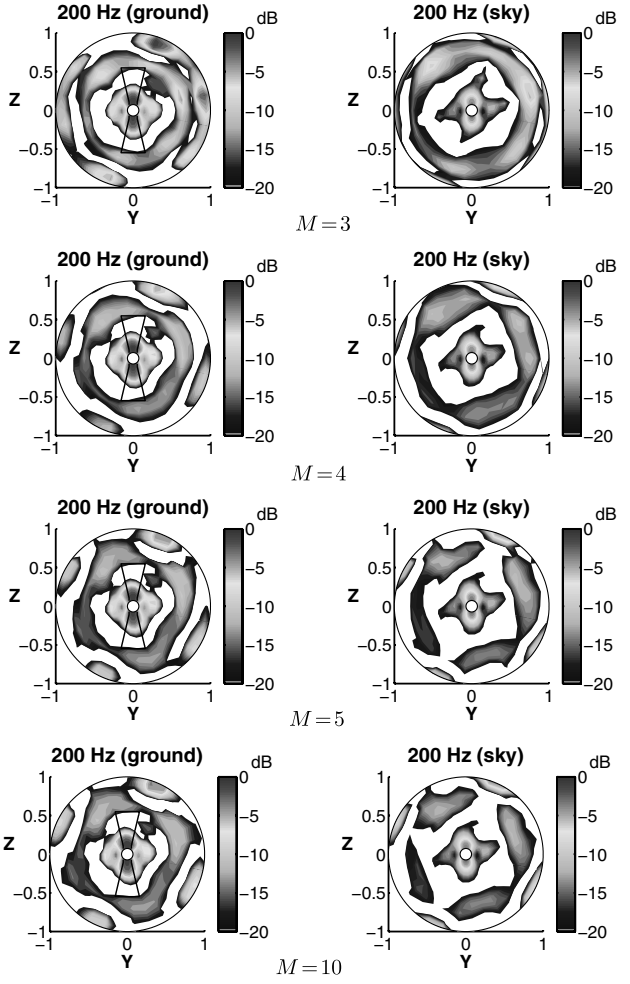

Fig. 11 CB maps computed with different values of the azimuthal truncation order M. Launcher at 0 m above the pad.

Downloaded by UNIVERSITY OF TENNESSEE on March 18, 2013 | http://arc.aiaa.org | DOI: 10.2514/1.J051479

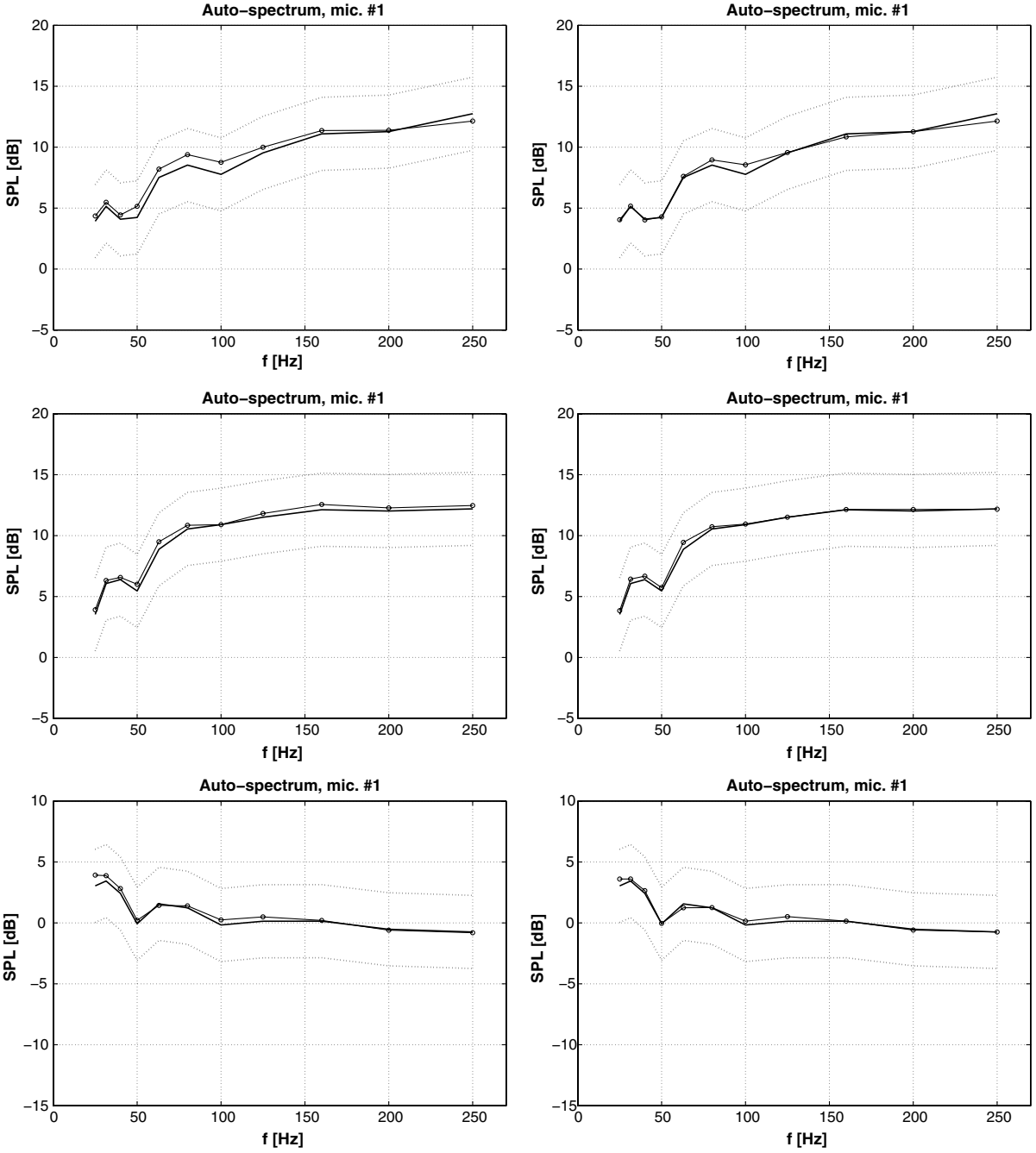

Fig. 12 Wall pressure spectra at microphone 1 referred to an arbitrary level. Launcher at 0 m (top), 10 m (middle) and 75 m (top) above the pad. On the left results obtained using the analytical plane wave formulation, on the right results obtained using the FEM elementary fields. Measurements (thick lines), measurements ±3 dB (dotted lines), predicted spectra (symbols).

Downloaded by UNIVERSITY OF TENNESSEE on March 18, 2013 | http://arc.aiaa.org | DOI: 10.2514/1.J051479

together with the ±3 dB curves that constitutes the design tolerance for the fairing electronic systems. The spectra are predicted with an error not exceeding 1 dB, that is less than the typical design tolerance. Interestingly, the accuracy of the prediction is not affected by the functional basis used to model the acoustic propagation: very similar results have been obtained by using the analytical and the numerical acoustic scattering model. Moreover, the accuracy is preserved down to the minimum frequency and it is not affected by the Rayleigh resolution limit. This result does not comply with the observation made by Panda and Mosher [13] who reported a fair resolution close to the Rayleigh limit.

Predicted cross-spectra between microphone 1 and other ones for the launcher altitude of 0 m are plotted in Fig. 13. Results are presented by comparing the predicted magnitude with the measured one, and by plotting the absolute value of the difference between the predicted and measured phase. It can be observed that the magnitude error is always within the design tolerance of ±3 dB in the whole frequency range; the phase error reaches in some cases the very high value of about 180 deg (C_{13}), but rarely exceeds 60 deg. Again, the accuracy of the prediction does not depend on the employed scattering model. Other results are reported in [25] (all microphone combinations, all launcher altitudes).

On the base of the presented results, it can be concluded that the SEM deconvolution method is quite robust in predicting the cross-spectra magnitude, but leads to significant phase errors. Further studies are necessary to increase the robustness of the inverse method in the phase prediction. In particular, different deconvolution methods will be employed [10,26] and the effects due to the assumption of uncorrelated plane waves will be investigated.

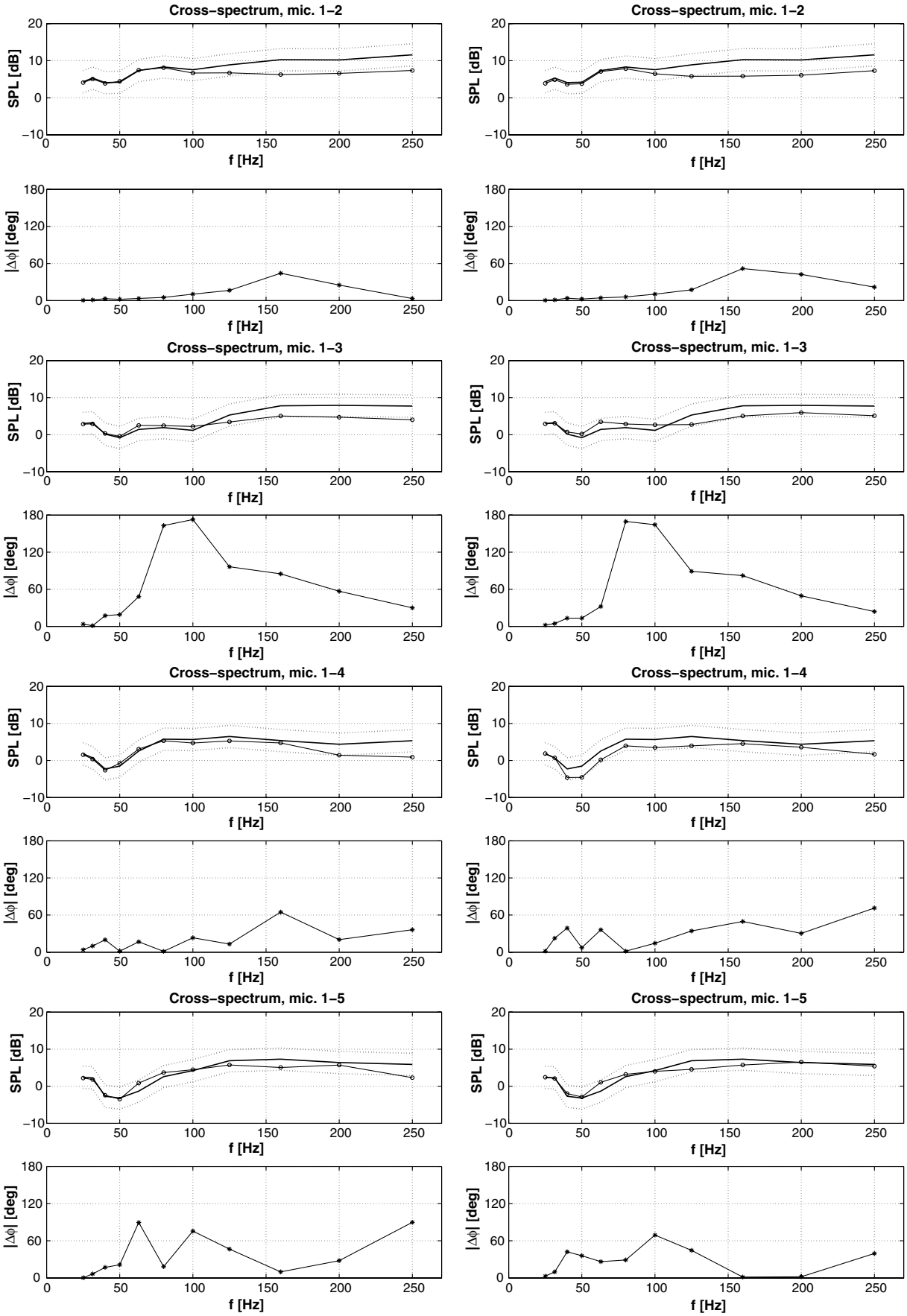

Fig. 13 Wall pressure cross-spectra. Launcher at 0 m above the pad. Analytical formulation on the left, numerical on the right. Measurements (thick lines), measurements ±3 dB (dotted lines), predicted cross-spectra (symbols).

Downloaded by UNIVERSITY OF TENNESSEE on March 18, 2013 | http://arc.aiaa.org | DOI: 10.2514/1.J051479

VII. Conclusions

In this work a beam-forming technique has been presented that permits to localize the sources of aerodynamic noise generated during the firing of a space launcher mock-up. The technique is based on the use of a steering-vector tailored to the specific acoustic problem and that reproduces the effects of plane waves impinging on the rocket structure from different directions. Two sets of functional bases have been used: the first one is constituted by analytical solutions based on the assumption that the rocket can be locally modeled as an infinite cylinder, the second one has been determined by solving numerically, through a FEM technique, the scattering problem for the real launcher geometry. These two acoustic models have been shown to be mutually consistent and to provide very similar source localizations results in the addressed frequency range of 25–250 Hz. A noise deconvolution procedure has been also validated by comparing the predicted noise spectra and cross-spectra at one location on the launcher with the ones computed from the measured signals. Again, as for the beam-forming results, no significant differences have been observed between the analytical and the numerical acoustic models. Moreover, the deconvolution algorithm has proven to be sufficiently robust in terms of magnitude, but not in phase. Further studies are therefore necessary to fix this problem. The present analysis has been conducted in a quite low-frequency range, due to the spatial aliasing limit of the employed microphone array. It is reasonably expected that higher frequency analyses, as required by a complete vibroacoustic analysis of the launcher fairing, would take advantage of the more accurate modeling of the wave scattering effects enabled by the FEM propagation model.

Acknowledgment

The noise measurements on the Vega scale mock-up have been carried out by European Launch Vehicle/AVIO in the framework of the national project CAST funded by the Italian Space Agency.

References

[1] Pavish, D. L., and Deese, J. E., "CFD Analysis of Unsteady Ignition Overpressure Effects on Delta II and III Launch Vehicles," AIAA Paper 2000-3922, 2000.

[2] Gély, D., Élias, G., Bresson, C., Foulon, H., Radulovic, S., and Roux, P., "Reduction of Supersonic Jet Noise—Application to the Ariane 5 Launch Vehicle," AIAA Paper 2000-2026, 2000.

[3] Eldred, K. M., "Acoustic Loads Generated by the Propulsion System," NASA SP-8072, June 1971.

[4] Candel, S., "Analysis of the Sound Field Radiated by the Ariane Launch Vehicle During Lift-Off," *La Recherche Aerospatiale*, Vol. 1983, No. 6, March 1971, pp. 17–33.

[5] Varnier, J., "Simplied Approach of Jet Aerodynamics with a View to Acoustics," *AIAA Journal*, Vol. 44, No. 7, July 2006, pp. 1690–1694. doi:10.2514/1.5087

[6] Casalino, D., Barbarino, M., Genito, M., and Ferrara, V., "Hybrid Empirical/Computational Aeroacoustics Methodology for Rocket Noise Modeling," *AIAA Journal*, Vol. 47, No. 6, June 2009, pp. 1445–1460. doi:10.2514/1.38634

[7] Alestra, S., Terrasse, I., and Troclet, B., "Inverse Method for Identification of Acoustic Sources at Launch Vehicle Liftoff," *AIAA Journal*, Vol. 41, No. 10, Oct. 2003, pp. 1980–1987. doi:10.2514/2.7318

[8] Morshed, M., Investigation of External Acoustic Loadings on a Launch Vehicle Fairing During Lift-Off, Ph.D. Thesis, Univ. of Adelaide, School of Mechanical Engineering, Australia, 2008.

[9] Höogbom, J. A., "Aperture Synthesis with a Non-Regular Distribution of Interferometer Baselines," *Astronomy and Astrophysics Supplement Series*, Vol. 15, 1974, pp. 417–426.

[10] Sijtsma, P., "CLEAN Based on Spatial Source Coherence," *International Journal of Aeroacoustics*, Vol. 6, No. 4, 2007, pp. 357–374. doi:10.1260/147547207783359459

[11] Blacodon, D., and Élias, G., "Level Estimation of Extended Acoustic Sources Using a Parametric Method," *Journal of Aircraft*, Vol. 41, No. 6, 2004, pp. 1360–1369. doi:10.2514/1.3053

[12] Brooks, T. F., and Humphreys, W. M., "A Deconvolution Approach for the Mapping of Acoustic Sources (DAMAS) Determined from Phased Microphone Array," *Journal of Sound and Vibration*, Vol. 294, Nos. 4–5, 2006, pp. 856–879. doi:10.1016/j.jsv.2005.12.046

[13] Panda, J., and Mosher, M., "Use of a Microphone Phased Array to Determine Noise Sources in Rocket Plumes," AIAA Paper2011-974, 2011.

[14] Gély, D., Élias, G., Mascanzoni, F., and Foulon, H., "Experimental Acoustic Characterization of the VEGA Launch Vehicle at Lift-Off," *6th International Symposium on Launchers Technologies*, Centre National d'Etudes Spatiales, Munich, Germany, Nov. 2005.

[15] Casalino, D., "Benchmarking of Different Wave Models for Sound Propagation in Non-Uniform Flows," *Procedia Engineering*, Vol. 6, March 2010, pp. 163–172. doi:10.1016/j.proeng.2010.09.018

[16] Casalino, D., "Finite Element Solutions of a Third-Order Wave Equation for Sound Propagation in Sheared Flows," AIAA Paper 2010-3762, June 2010.

[17] Li, T.-B., and Ueda, M., "Sound Scattering of a Plane Wave Obliquely Incident on a Cylinder," *Journal of the Acoustical Society of America*, Vol. 86, No. 6, December 1989, pp. 2363–2368. doi:10.1121/1.398444

[18] Morse, P. M., and Ingard, K. U., *Theoretical Acoustics*, McGraw–Hill, New York, 1968.

[19] Casalino, D., Barbarino, M., and Visingardi, A., "Simulation of Helicopter Community Noise in Complex Urban Geometry," *AIAA Journal*, Vol. 49, No. 8, 2011, pp. 1614–1624. doi:10.2514/1.J050774

[20] Casalino, D., and Barbarino, M., "Optimization of a Single Slotted Lined Flap for Airframe Noise Reduction," AIAA Paper 2011-2730, June 2011.

[21] Casalino, D., and Barbarino, M., "A Stochastic Method for Airfoil Self-Noise Computation in Frequency-Domain," *AIAA Journal*, Vol. 49, No. 11, Nov. 2011, pp. 2453–2469. doi:10.2514/1.J050773

[22] Astley, R. J., and Eversman, W., "A Finite Element Method for Transmission in Non-Uniform Ducts Without Flow: Comparison with the Method of Weighted Residuals," *Journal of Sound and Vibration*, Vol. 57, No. 3, 1978, pp. 367–388. doi:10.1016/0022-460X(78)90317-6

[23] Mascanzoni, F., and Contini, C., "The Acoustic Environment of the VEGA LV at Lift-Off: the BEAT Acoustic Experimental Test Facility," *6th International Symposium on Launchers Technologies*, Centre National d'Etudes Spatiales, Munich, Germany, Nov. 2005.

[24] Lawson, C. L., and Hanson, R. J., *Solving Least Squares Problems*, Prentice–Hall, Englewood Cliff, NJ, 1974.

[25] Casalino, D., Santini, S., Genito, M., and Ferrara, V., "Rocket Noise Sources Localization through a CAA-Based Beam-Forming Technique," AIAA Paper 2011-2722, June 2011.

[26] Ravetta, P., Burdisso, R., and Wing, F., "Noise Source Localization and Optimization of Phased-Array Results," *AIAA Journal*, Vol. 47, No. 11, 2009, pp. 2520–2533. doi:10.2514/1.38073

C. Bailly
Associate Editor

Downloaded by UNIVERSITY OF TENNESSEE on March 18, 2013 | http://arc.aiaa.org | DOI: 10.2514/1.J051479